



Structure and compositional trends in alkali-metal containing titanium and vanadium oxide chalcogenides and the new van der Waals phase $\text{Ti}_2\text{Te}_2\text{O}$

Nicola D. Kelly, Simon J. Clarke *

Inorganic Chemistry Laboratory, University of Oxford, South Parks Road, Oxford, OX1 3QR, Oxfordshire, UK

ARTICLE INFO

Keywords:

X-ray diffraction

Heteroanionic

Layered materials

ABSTRACT

We report the solid-state synthesis of all eighteen layered oxide chalcogenides in the structural family AM_2Q_2O ($A = \text{K/Rb/Cs}$; $M = \text{Ti/V}$; $Q = \text{S/Se/Te}$), allowing the determination of trends in composition and reactivity within the series. All materials are isostructural, crystallising in the primitive tetragonal space group $P4/mmm$ as reported previously for five compounds in the series. The titanium or vanadium ions have intermediate valency on a single crystallographic site, leading to temperature-independent paramagnetism and correlated electronic behaviour which is influenced by the compositional variation. Furthermore, the alkali metal ions in $\text{KTi}_2\text{Te}_2\text{O}$ and $\text{RbTi}_2\text{Te}_2\text{O}$ can be removed by oxidative deintercalation using H_2O at room temperature to produce a new metastable van der Waals layered phase, $\text{Ti}_2\text{Te}_2\text{O}$. During the deintercalation reaction the oxide chalcogenide layers undergo a relative shift by (0.5,0.5) in the ab plane such that $\text{Ti}_2\text{Te}_2\text{O}$ is body-centered with space group $I4/mmm$.

1. Introduction

Mixed-anion compounds in the solid state offer the opportunity for more complex crystal structures than those typically observed in simple oxides, sulfides or other single-anion materials [1–3]. Long-range ordering of anions with different chemistries (sizes and electronegativities) is common. In particular, layered structures are often formed owing to the anions having different preferences for bonding with different cations [4–6]. Layered mixed-anion crystal structures can produce unusual physical phenomena such as two-dimensional magnetic ordering [7–9], metamagnetism [10], or superconductivity [11,12].

In 2016, Valldor et al. reported the synthesis of two layered mixed-anion compounds: a vanadium oxide sulfide $\text{CsV}_2\text{S}_2\text{O}$ [13] and an isostructural titanium oxide telluride $\text{Cs}_{1-x}\text{Ti}_x\text{Te}_2\text{O}$ ($x \approx 0.2$) [14]. In 2018, Lin et al. synthesised $\text{CsV}_2\text{Se}_2\text{O}$ [15] and Ablimit et al. synthesised $\text{Rb}_{1-\delta}\text{V}_\delta\text{Te}_2\text{O}$ ($\delta \approx 0.2$) [16]. $\text{KV}_2\text{Se}_2\text{O}$ was reported in 2021 by Guo et al. as a secondary phase during the synthesis of KV_3Se_3 [17], although its physical properties were not measured. These compounds can be represented by the general formula AM_2Q_2O where $A = \text{K/Rb/Cs}$, $M = \text{Ti/V}$, $Q = \text{S/Se/Te}$.

The structure of AM_2Q_2O is shown in Fig. 1. It contains edge-sharing $\text{trans-MQ}_4\text{O}_2$ octahedra which form an $M_2\text{O}$ square layer, described as anti- CuO_2 -type with reference to the layered cuprate high-

temperature superconductors [11,12,15,16,18]. Such coordination of oxide anions by 4 metal cations in a square-planar arrangement is rather unusual outside of this structure type, particularly among oxide chalcogenides where tetrahedral or trigonal coordination is more common, e.g. LnO_2Te [19] or $(\text{La/Nd})\text{CrOS}_2$ [20]. The alkali metal cations are situated in 8-coordinate square prismatic positions between the transition metal-oxide chalcogenide layers. This structure type also occurs in the barium titanium oxide pnictides $\text{BaTi}_2\text{As}_2\text{O}$ [21], $\text{BaTi}_2\text{Bi}_2\text{O}$ [12] and $\text{BaTi}_2\text{Sb}_2\text{O}$ [11], in which the divalent chalcogenide anions have been replaced by trivalent pnictide anions and K^+ replaced by Ba^{2+} . Two superconducting regions of the phase diagrams [22] and superconductivity could also be enhanced by aliovalent partial substitution of alkali metal ions for Ba^{2+} (i.e. hole-doping) in $\text{BaTi}_2\text{Sb}_2\text{O}$ [23–26]. Applying chemical pressure to the related oxide chalcogenides, by complete or partial substitution on the A , M and/or Q sites of AM_2Q_2O , is also expected to produce interesting electronic behaviour through the balance of localised versus itinerant $3d$ -electrons [15]. In this work we report the solid-state synthesis of thirteen new compounds within the AM_2Q_2O phase space which enables the structural and compositional trends in the series to be revealed. The new compounds are isostructural with the five previously reported members of this family and are air- and water-sensitive, temperature-independent paramagnets.

* Corresponding author.

E-mail address: simon.clarke@chem.ox.ac.uk (S.J. Clarke).

<https://doi.org/10.1016/j.jssc.2023.124276>

Received 26 May 2023; Received in revised form 18 July 2023; Accepted 9 August 2023

Available online 19 August 2023

0022-4596/© 2023 The Author(s). Published by Elsevier Inc. This is an open access article under the CC BY license (<http://creativecommons.org/licenses/by/4.0/>).

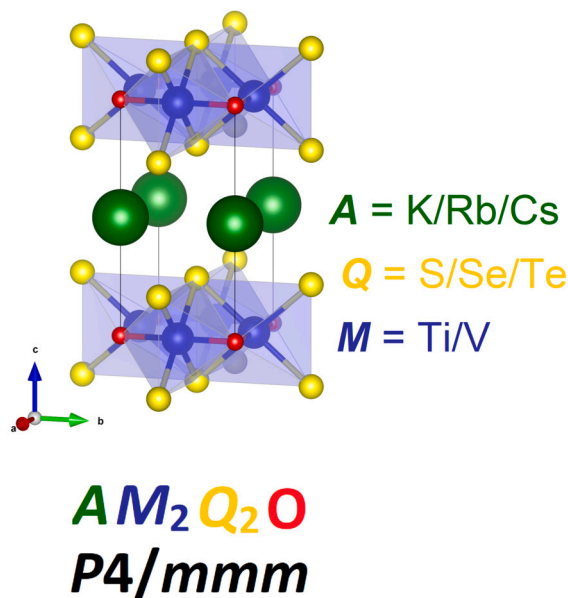


Fig. 1. Crystal structure of AM_2Q_2O .

Incorporation of smaller 3d transition metals into the edge-sharing octahedral M_2Q_2O structural motif occurs quite frequently, including $M = Fe$ [6,27–32], Mn [32], and Co [8]. However, all examples cited above contain either double alkali metal, e.g. Na_2 , or antiperovskite-type layers, e.g. $(LaO)_2$, $(BaF)_2$, rather than a single cationic A layer. The 1221 AM_2Q_2O structure type has been reported with $M = Fe$ only in the high-pressure polymorphs of $BaFe_2S_2O$ [18] and $BaFe_2Se_2O$ [33], whereas samples synthesised at ambient pressure adopt a different crystal structure containing spin ladders of tetrahedrally coordinated Fe^{2+} [34]. Our attempts to introduce Cr onto the M -site of AM_2Q_2O were unsuccessful, although $Sr_2Cr_3O_3As_2$ ($\equiv Sr_2CrO_2Cr_2OAs_2$) was recently reported with the first known example of $M = Cr^{3+}$ in the M_2Q_2O layers [35]. The layered tetragonal AM_2Q_2O structure clearly occupies a complex phase space with many competing structure types.

Materials with the AM_2Q_2O structure type also offer the opportunity for soft-chemical manipulation via intercalation or deintercalation. For example, the alkali metal ions in CsV_2Se_2O and $Rb_{1-\delta}V_2Te_2O$ could be completely deintercalated using iodine or water respectively to produce metastable van der Waals compounds V_2Se_2O or V_2Te_2O respectively [15,36]. These reactions are topochemical processes in which the structure of the M – Q – O layers is preserved while alkali metal ions are extracted. However, the reactions necessitate a relative shift of those layers in the ab plane and thus a change in the space group symmetry from primitive $P4/mmm$ to body-centered $I4/mmm$. We here report the synthesis of a novel van der Waals layered material Ti_2Te_2O , isostructural with V_2Te_2O and V_2Se_2O , using a facile soft chemical approach starting from the new compositions KTi_2Te_2O or $RbTi_2Te_2O$.

2. Experimental methods

All sample preparation and manipulation was carried out in an argon-filled glovebox. The precursor VSe_2 was synthesised on a 2 g scale from a 1:2 molar ratio of V powder (99.5%, Alfa Aesar) and Se powder (99.999%, Alfa Aesar) following the procedure given in reference 15. The reagents were ground together with a pestle and mortar, pressed into a 13 mm diameter pellet under 4 tonnes pressure and flame-sealed into an evacuated silica tube. The tube was heated in a muffle furnace at $1^\circ C\ min^{-1}$ to $700^\circ C$, held at that temperature for 24 h, then cooled naturally to room temperature by switching off the furnace. The resultant dark grey solid was found to be phase-pure by laboratory powder X-ray diffraction (PXRD).

Samples of AM_2Q_2O were synthesised on the 0.5–1.0 g scale from appropriate stoichiometric mixtures of K , Rb or Cs metal, TiO_2 or V_2O_5 , Ti or V , and VSe_2 , S or Te (all reagents $\geq 99.5\%$, Alfa Aesar), in a procedure adapted from reference 16. The alkali metal was weighed into an alumina crucible and the remaining powdered reagents poured on top. The crucible was placed in a long silica tube, a lid or a second crucible was placed on top, and the tube was flame-sealed under dynamic vacuum. During sealing, the base of the tube was submerged in liquid N_2 to prevent evaporation of volatile reagents. The sealed tubes were heated in muffle furnaces at $1^\circ C\ min^{-1}$ to $300^\circ C$ (Se , Te compounds) or $400^\circ C$ (S compounds), held at that temperature for 12 h, then cooled naturally to room temperature by switching off the furnace. The samples were transferred into the glovebox, ground in a pestle and mortar, pressed into pellets, sealed into new silica tubes and reheated at $700^\circ C$ (Se , Te compounds) or $800^\circ C$ (S compounds) for 24 h with the same heating and cooling rates. The products were black powders.

Powder X-ray diffraction (PXRD) was carried out at room temperature on a Bruker D8 Advance Eco diffractometer with $Cu\ K\ \alpha$ radiation, $\lambda = 1.541\ \text{\AA}$. The sample was loaded onto a lightly greased glass slide and mounted in a custom-made airtight sample holder with Mylar® windows. The measurement conditions were: angle ($^\circ$) $10 \leq 2\theta \leq 70$; step size 0.01° ; time per step 0.25 s (total scan time 25 minutes); fixed slits 0.5 mm. Subsequently, synchrotron PXRD was carried out at the I11 beamline, Diamond Light Source, Didcot, UK [37], with a wavelength of $\lambda \approx 0.82\ \text{\AA}$ (calibrated precisely at the start of each beamtime session using a Si standard). Samples were mixed 1:1 by volume with ground glass to reduce beam absorption and packed into borosilicate capillaries of diameter 0.3 mm (measurements at or below room temperature) or quartz capillaries of diameter 0.5 mm (measurements above room temperature). Diffraction patterns were collected using the Position Sensitive Detector (PSD). For Ti_2Te_2O , diffraction patterns were also collected on warming from 100 K to 500 K using a cryostream and from room temperature to $900^\circ C$ using a hot air blower, each with a ramp rate of $12^\circ C\ min^{-1}$. All Rietveld refinement [38] was carried out using the program TOPAS-Academic V7 [39].

Soft chemical reactions were carried out on a Schlenk line. For each reaction with water, a cannula was used to transfer approximately 5 mL degassed, deionised water into a Schlenk tube containing 100 mg of the parent material. The reaction was stirred for 4 h at room temperature under a static N_2 atmosphere. After this time, the water was removed by filtration under flowing N_2 and the sample washed twice with anhydrous tetrahydrofuran. The resultant dark grey solids were dried under vacuum for 15 minutes before being transferred into a glovebox for further manipulation and characterisation.

For electronic characterisation of the compounds prepared at high temperatures, samples were pressed into pellets of 5 mm diameter under 2 tonnes pressure and annealed under vacuum for 12 h at $700^\circ C$. Resistance was measured at room temperature inside the argon-filled glovebox using a two-probe method with a digital multimeter.

Magnetic measurements were made using a Quantum Design MPMS-XL or MPMS-3 SQUID magnetometer. Powder samples of mass 20–30 mg (accurately measured in each case) were placed in gelatine capsules and inserted into plastic straws before being attached to the sample stick and lowered into the instrument. Magnetic susceptibility $\chi \approx M/H$ was measured on warming from 2 K in both the zero-field-cooled (ZFC) and field-cooled (FC) regimes in an applied magnetic field of 10 kOe (1 T). Isothermal magnetisation was measured at 300 K to $\pm 5\ T$; no hysteresis was observed but there was some nonlinearity at low fields, indicating the presence of minor magnetic impurities.

3. Results and discussion

3.1. Crystal structure trends in the series AM_2Q_2O

Rietveld refinements [38] were carried out on the synchrotron PXRD data in space group $P4/mmm$ using initial atomic positions taken from

Table 1

Refined crystallographic information for AM_2Q_2O powder samples, from Rietveld refinement of room temperature synchrotron PXRD data. The results for CsV_2S_2O [13], KV_2Se_2O [17], CsV_2Se_2O [15], RbV_2Te_2O [16] and $CsTi_2Te_2O$ [14] agree well with literature reports.

Composition	$a/\text{\AA}$	$c/\text{\AA}$	z_Q	occ_A
KV_2S_2O	3.900606(8)	6.98287(2)	0.2323(1)	1.000(2)
KTi_2S_2O	3.94418(2)	7.13966(8)	0.2316(2)	0.972(3)
RbV_2S_2O	3.930690(10)	7.17101(3)	0.2203(2)	0.944(1)
$RbTi_2S_2O$	3.93829(2)	7.35310(7)	0.2307(2)	1.000(2)
CsV_2S_2O	3.94095(4)	7.48852(13)	0.2139(6)	1.000(8)
$CsTi_2S_2O$	3.999038(10)	7.60279(3)	0.21603(14)	0.983(2)
KV_2Se_2O	3.966342(7)	7.34854(2)	0.23612(9)	1.000(3)
KTi_2Se_2O	3.95251(4)	7.54058(14)	0.2462(2)	1.000(4)
RbV_2Se_2O	3.965218(9)	5.75947(3)	0.22688(10)	0.975(2)
$RbTi_2Se_2O$	4.00809(3)	7.70860(9)	0.23283(10)	1.000(2)
CsV_2Se_2O	4.007704(6)	7.87574(2)	0.21751(8)	0.992(2)
$CsTi_2Se_2O$	4.06663(3)	7.96911(7)	0.22015(13)	0.995(2)
KV_2Te_2O	4.027171(9)	8.22706(3)	0.23598(7)	0.773(5)
KTi_2Te_2O	4.06693(3)	8.36954(8)	0.24124(9)	0.720(3)
RbV_2Te_2O	4.043609(9)	8.44999(3)	0.22820(5)	0.830(2)
$RbTi_2Te_2O$	4.06742(3)	8.62472(10)	0.23086(11)	0.685(3)
CsV_2Te_2O	4.05798(2)	8.78655(6)	0.21797(11)	0.874(2)
$CsTi_2Te_2O$	4.08883(4)	8.99389(12)	0.22129(8)	0.641(1)

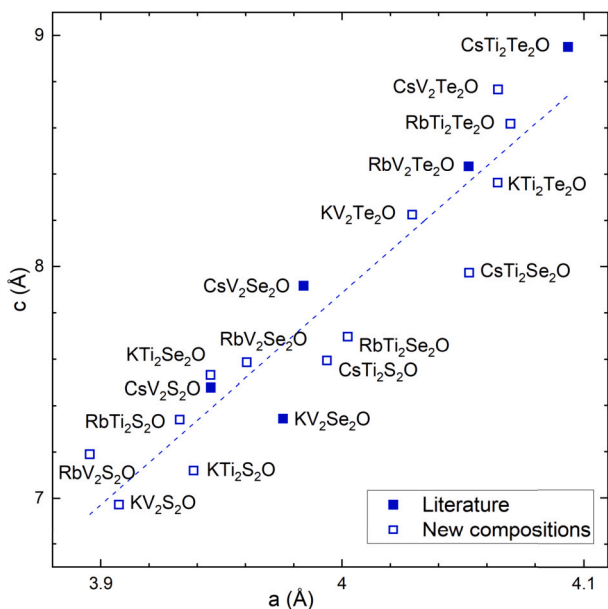


Fig. 2. Lattice parameters a and c of AM_2Q_2O materials in the literature (filled symbols) [13–17] and this work (open symbols). The dashed line is a least-squares fit.

the literature report of $Rb_{1-x}V_2Te_2O$ [16]. The atomic positions are: K/Rb/Cs – $1b$ (0,0,0.5); Ti/V – $2f$ (0,0.5,0); S/Se/Te – $2h$ (0.5,0.5, z); O – $1a$ (0,0,0). The systematic zero point error, unit cell parameters, chalcogen z -coordinate and fractional occupancy of the alkali metal site (constrained to lie between 0 and 1) were refined. Isotropic thermal displacement parameters were fixed at 1 \AA^2 for all atoms [40] because allowing for free refinement led to variable and/or unphysical results, i.e. zero or negative values. The refined parameters are given in Table 1 and graphically in Fig. 2. A representative refinement is given in Fig. 3 and refinements for all compositions may be found in Figures S2–S4.

Minor impurity phases were present in the Se and Te samples as judged by PXRD. For the vanadium oxide tellurides, these were identified as Te, V_2O_3 , and the quasi-1D compounds $AV_3Te_3O_8$ [17], whereas the structurally related KV_3Se_3 [17] was not observed in our synthesis of KV_2Se_2O . The oxide selenides typically contained small amounts

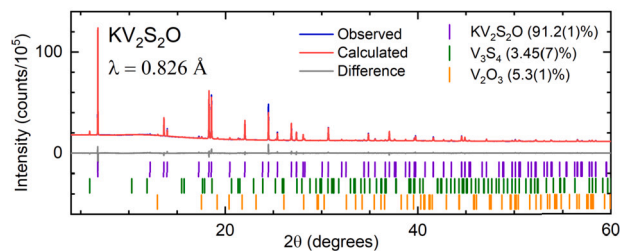


Fig. 3. Rietveld refinement of synchrotron PXRD data for KV_2S_2O . Blue lines: observed intensities, red: calculated, grey: difference. Tick marks show the positions of Bragg reflections for KV_2S_2O (purple), V_3S_4 (green) and V_2O_3 (orange).

of V_2O_3 or Ti_2O_3 as a secondary phase. Regrinding and reheating at $T \geq 700^\circ\text{C}$ improved phase purity only to a small extent. Various alternative synthetic routes were tested, e.g. omitting the low-temperature preheat stage or starting from elemental Se rather than VSe_2 , but these did not result in increased phase purity.

For the oxide sulfides, it was found that a higher temperature of 400°C was required for the preheat stage in order to prevent the intermediate compound becoming stuck to the crucibles, presumably due to the formation of molten intermediate material. However, poor phase purity was still observed after heating at 700°C ; sample purity improved at the higher synthesis temperature of 800°C but generally remained much lower than for the Se and Te analogues. Subsequent reheating at 800°C reduced the amounts of unknown phases at the cost of increasing amounts of the secondary phase $A_xM_6S_8$ [41]. Heating to $T \geq 900^\circ\text{C}$ decomposed the target materials, forming V_2O_3 and $A_xM_6S_8$.

The Rietveld refinements on nominally stoichiometric AM_2Q_2O samples indicated sample-dependent alkali metal deficiencies of up to 35%, likely owing in part to the use of volatile elemental alkali metal as a starting material. We made repeated attempts to synthesise each composition; Table 1 gives the lattice parameters for a representative sample of each compound. We found that the oxide tellurides always showed a large alkali metal deficiency, consistent with the literature on $Cs_{1-x}Ti_2Te_2O$ [14] and $Rb_{1-x}V_2Te_2O$ [16] and the ease of oxidation of telluride. The selenides and sulfides varied in a less systematic manner, but it was possible to achieve close to full occupancy of the alkali metal sites.

To obtain further insight into the possible range of x , we synthesised samples of $K_{1-x}Ti_2Se_2O$ with target stoichiometry $x = 0$ to $x = 0.3$ in steps of 0.05 in x . However, in each case the reaction formed a phase with close to full potassium occupancy, alongside unidentified impurity phases which are assumed to contain the remaining Ti, Se and O. There was a non-linear relationship between the target and refined x and the maximum value of refined x was 0.11 (Fig. S5), suggesting that the more potassium-deficient compositions are only kinetically accessible (see later sections 3.2 and 3.3).

This work shows that all of the $3 \times 2 \times 3 = 18$ AM_2Q_2O phases ($A = K/Rb/Cs$, $M = Ti/V$, $Q = S/Se/Te$) are accessible, albeit that significant alkali metal non-stoichiometry is typically found for $Q = Te$, likely owing to the ease of oxidation of telluride [42]. Synthesis of the target 1221 phases “ NaV_2Se_2O ” and “ LiV_2Se_2O ” was unsuccessful, resulting in a mixture of binary compounds. This is likely the result of the Na^+ and Li^+ ionic radii being too small to occupy the 8-coordinate sites in the AM_2Q_2O structure. For example, Na^+ ions in the related compound $Na_2Fe_2S_2O$ occupy 4-coordinate positions [6].

3.2. Reactions with water

Samples of each composition were reacted with deionised H_2O in a Schlenk tube under N_2 at room temperature. The purpose of this investigation was to search for new van der Waals compounds isostructural with V_2Te_2O which was produced using this method [36]. Most of the AM_2Q_2O materials are reactive towards water, with the typical behaviour appearing to depend most strongly on the identity of Q ,

Table 2

Results of reactions of AM_2Q_2O powder samples with degassed, deionised water under a nitrogen atmosphere, and with moist air in the lab.

Parent material	Reaction with H ₂ O under N ₂	Reaction with moist air
KV ₂ S ₂ O	Partial deintercalation of K ⁺ ions: $x = 0$ to $x' = 0.171(12)$.	Peak broadening, decomposition through partial loss of K ⁺ (Fig. S6).
KTi ₂ S ₂ O	Partial deintercalation of K ⁺ ions: $x = 0$ to $x' = 0.288(7)$.	Partial loss of K ⁺ (Fig. S7).
RbV ₂ S ₂ O	Partial deintercalation of Rb ⁺ ions: $x = 0.073(6)$ to $x' = 0.243(5)$.	Peak broadening, decomposition through partial loss of Rb ⁺ (Fig. S8).
RbTi ₂ S ₂ O	No reaction.	Peak broadening, slow decomposition through partial loss of Rb ⁺ .
CsV ₂ S ₂ O	No reaction.	Decomposition over a few days, forming V ₂ O ₃ .
CsTi ₂ S ₂ O	No reaction.	No reaction after 2 weeks.
KV ₂ Se ₂ O	Partial deintercalation of K ⁺ ions: $x = 0$ to $x' = 0.324(12)$.	Peak broadening, decomposition through partial loss of K ⁺ .
KTi ₂ Se ₂ O	Partial deintercalation of K ⁺ ions: $x = 0$ to $x' = 0.251(14)$.	Peak broadening, decomposition through partial loss of K ⁺ .
RbV ₂ Se ₂ O	Partial deintercalation of Rb ⁺ ions: $x = 0.061(3)$ to $x' = 0.204(6)$.	Peak broadening, slow decomposition into RbVO ₃ and Se.
RbTi ₂ Se ₂ O	No reaction.	Peak broadening, slow decomposition through partial loss of Rb ⁺ .
CsV ₂ Se ₂ O	No reaction.	No reaction after 1 month.
CsTi ₂ Se ₂ O	No reaction.	No reaction after 2 weeks.
KV ₂ Te ₂ O	Complete deintercalation of K ⁺ to form V ₂ Te ₂ O.	Decomposed to V ₂ Te ₂ O and Te after 1 day (Fig. S9).
KTi ₂ Te ₂ O	Complete deintercalation of K ⁺ to form Ti ₂ Te ₂ O.	Decomposed to elemental Te after 1 day.
RbV ₂ Te ₂ O	Complete deintercalation of Rb ⁺ to form V ₂ Te ₂ O.	Decomposed to V ₂ Te ₂ O, Te and RbVO ₃ over the course of 1 week.
RbTi ₂ Te ₂ O	Complete deintercalation of Rb ⁺ to form Ti ₂ Te ₂ O.	Decomposed to elemental Te after 1 day.
CsV ₂ Te ₂ O	No reaction.	Decomposed to V ₂ Te ₂ O, Te and CsVO ₃ over the course of 1 week (Fig. S10).
CsTi ₂ Te ₂ O	No reaction.	Decomposed to elemental Te after 1 day.

followed by A, as detailed below and summarised in Fig. 6 (top) and Table 2.

PXRD and Rietveld refinement indicated that KV₂Te₂O and RbV₂Te₂O underwent complete deintercalation of the alkali metals to produce V₂Te₂O [36], while CsV₂Te₂O and CsTi₂Te₂O did not react. KTi₂Te₂O and RbTi₂Te₂O reacted with water to give a new layered material, Ti₂Te₂O, discussed further in section 3.5.

For the oxide selenides, CsV₂Se₂O, CsTi₂Se₂O and RbTi₂Se₂O were insensitive to water, while KV₂Se₂O, KTi₂Se₂O and RbV₂Se₂O each underwent partial removal of the A⁺ ions. The change in refined values of x was supported by changes in the relative peak intensities, with the 00 ℓ Bragg reflections becoming more intense as alkali metal ions were removed. At the same time, the c lattice parameter increases as some of the strong A⁺–Se²⁻ interlayer ionic interactions are replaced by weaker van der Waals interactions [43], and the a parameter decreases as vanadium or titanium ions are oxidised, shortening the M–O bonds which lie parallel to a . For example, the refined stoichiometry of K_{1- x} Ti₂Se₂O changed from $x = 0$ to $x' = 0.251(14)$ after reaction with H₂O and the lattice parameters were $a = 3.90605(17)$, $a' = 3.8949(2)$ (a decrease of 0.3%); $c = 7.5650(6)$, $c' = 7.6150(10)$ (an increase of 0.7%).

The oxide sulfides behaved in a similar way to the oxide selenides. CsV₂S₂O, CsTi₂S₂O and RbTi₂S₂O did not react with H₂O, although some unidentified secondary phases in the as-made samples were water-soluble and disappeared from the diffraction patterns after reaction with water. The A⁺ ions in the oxide sulfides KV₂S₂O, KTi₂S₂O and RbV₂S₂O were partially removed by water. For example, the Rb deficiency increased from $x = 0.056(1)$ in the parent Rb_{1- x} V₂S₂O to $x' = 0.243(5)$ in the daughter compound after reaction with H₂O. Peak broadening from parent to daughter samples was also observed as A⁺ ions were deintercalated from all three materials.

Overall, the deintercalation chemistry of these compounds appears rather complex. The results for all compositions are summarised in Table 2. We suggest that the large Cs⁺ ions in all A = Cs compositions of AM_2Q_2O are not removed by H₂O because they are large, leading to a diffuse positive charge which is less strongly solvated by water com-

pared with Rb⁺ or K⁺. Furthermore, complete removal of the A⁺ ions was observed only for Q = Te with A = K or Rb, M = Ti or V. However, the differences in reactivity within pairs of similar compounds, i.e. RbV₂S₂O/RbTi₂S₂O and RbV₂Se₂O/RbTi₂Se₂O, indicates that the reactivity cannot be explained solely by the strength of the alkali metal–chalcogenide bonding and the oxidisability of the transition metal must also play an important part.

3.3. Reactions with air

Air sensitivity was measured by removing the airtight lids from the XRD sample holders and collecting further diffraction patterns at set time intervals afterwards. Most of the AM_2Q_2O materials are air-sensitive with the typical behaviour appearing to depend most strongly on the identity of Q, followed by A, as detailed below and summarised in Fig. 6 (bottom) and Table 2. Additional details for selected air-exposed samples are available in Figures S6–S10.

The oxide tellurides are very unstable in air. KV₂Te₂O decomposed into V₂Te₂O [36] and elemental Te after only 1 day in moist air, while CsV₂Te₂O was entirely converted to V₂Te₂O, CsVO₃ and Te after 1 week, in contrast to its lack of reactivity with water in the absence of oxygen. RbV₂Te₂O decomposed similarly and on the same timescale as its Cs analogue, in agreement with the literature which states that it is “very air sensitive” [16]. All three titanium oxide tellurides had fully decomposed after 1 day in air leaving elemental Te, from oxidation of the telluride ions, as the only crystalline product. The differences in reactivity between air and degassed water (section 3.2) presumably reflect the more oxidising environment of moist air, which aids the oxidative deintercalation.

The oxide selenides are in general less reactive than the tellurides. CsV₂Se₂O [15] and CsTi₂Se₂O appeared stable in air. KV₂Se₂O (see later), RbV₂Se₂O and RbTi₂Se₂O decomposed slowly with partial loss of the alkali metal ions; after 1 month, the sample of RbV₂Se₂O contained similar amounts of both the parent Rb_{1- x} V₂Se₂O ($x = 0.05$) and a

daughter phase with broadened peaks and a refined value of x of 0.21. This suggests that kinetic factors also control the reactivity.

An *in situ* diffraction experiment was carried out on $\text{KTi}_2\text{Se}_2\text{O}$. The sample was loaded onto an XRD holder without the airtight lid, removed from the glovebox and immediately loaded into the diffractometer. A continuous series of 30-minute scans were collected over a 60 h period and sequential Rietveld refinement was used to analyse the results. Upon reaction with moist air, partial decomposition occurred as evidenced by the changes in phase fractions of the main phase and elemental Se, Fig. 4(a). At the same time potassium ions were extracted from the main phase, first rapidly and then more slowly, Fig. 4(b). The extent of deintercalation appears to level off at approximately 30% within the time constraints of this experiment, i.e. a limit of $\text{K}_{1-x}\text{Ti}_2\text{Se}_2\text{O}$ with $x = 0.3$, which is similar to the composition obtained in a direct reaction with water. Over the duration of the experiment, increasing x obtained by Rietveld refinement is correlated with increasing c and decreasing a , Fig. 4(c). These trends are rationalised by fewer interlayer ionic interactions and smaller (oxidised) Ti ions, as discussed above in section 3.2. The K-deficient phases produced in this experiment were not available under thermodynamic control at high temperatures (section 3.1).

Another *in situ* diffraction experiment was carried out on $\text{KV}_2\text{Se}_2\text{O}$ showing the same changes in lattice parameters (Fig. 5(a),(b)) and partial deintercalation of K^+ ions, consistent with the *ex situ* data. In this case, examination of the raw data showed clear evidence for overlapping peaks at intermediate timescales, i.e. coexistence of two $\text{K}_{1-x}\text{V}_2\text{Se}_2\text{O}$ phases with different x . This contrasts with the titanium analogue where there appeared to be a single phase with variable composition (Fig. 4). Rietveld refinement of the $\text{K}_{1-x}\text{V}_2\text{Se}_2\text{O}$ data after 60 h air exposure revealed a single daughter phase with $x = 0.442(7)$, Fig. 5(c). Sequential refinement was carried out over all scans and indicated that the weight fraction of parent phase decreased smoothly as the fractions of daughter phase and elemental Se increased. However, the overlapping peaks, coupled with significant peak broadening as the sample decomposed, prevented any further structural analysis.

The vanadium oxide sulfides $\text{KV}_2\text{S}_2\text{O}$ and $\text{RbV}_2\text{S}_2\text{O}$ reacted similarly to their analogous oxide selenides, decomposing through gradual loss of K^+ with evidence of two-phase behaviour (Figures S6 and S8). $\text{RbV}_2\text{S}_2\text{O}$ decomposed similarly to the Rb selenide but on a faster timescale. $\text{CsV}_2\text{S}_2\text{O}$ deteriorates slowly in air, in agreement with the literature [13], forming V_2O_3 . For the titanium compounds, an *in situ* diffraction experiment on $\text{KTi}_2\text{S}_2\text{O}$ (Fig. S7) showed very similar (single-phase) behaviour to $\text{KTi}_2\text{Se}_2\text{O}$ in air. $\text{RbTi}_2\text{S}_2\text{O}$ appeared to lose Rb^+ very slowly, while $\text{CsTi}_2\text{S}_2\text{O}$ had no observable reaction.

The reactions with air are believed to be driven chiefly by the presence of water vapour, owing to similarities with the observations on reaction with H_2O under an inert atmosphere (section 3.2). However, there are some significant differences in reactivity, as described in the preceding sections and illustrated graphically in Fig. 6. For example, $\text{V}_2\text{Te}_2\text{O}$ and $\text{Ti}_2\text{Te}_2\text{O}$ were both observed in the reactions of $\text{AM}_2\text{Q}_2\text{O}$ oxide tellurides with water, whereas only $\text{V}_2\text{Te}_2\text{O}$ was observed in the reactions with moist air, suggesting that $\text{Ti}_2\text{Te}_2\text{O}$ might be stable in H_2O but undergo further oxidation if O_2 is also present. Controlled reactions with dry O_2 could be carried out to investigate the reactivity in more detail. There may be electronic factors governing the single-versus two-phase behaviour in the titanium and vanadium compounds respectively and these could be probed by computation. Furthermore, these soft-chemical reactions may be kinetically controlled so varying the time and temperature of the reactions with water might shed light on some of these differences.

3.4. Electronic and magnetic properties

Electronic and magnetic characterisation was hampered by the high air-sensitivity of these materials (section 3.3), such that it was not feasible to carry out four-probe resistivity measurements as a function of

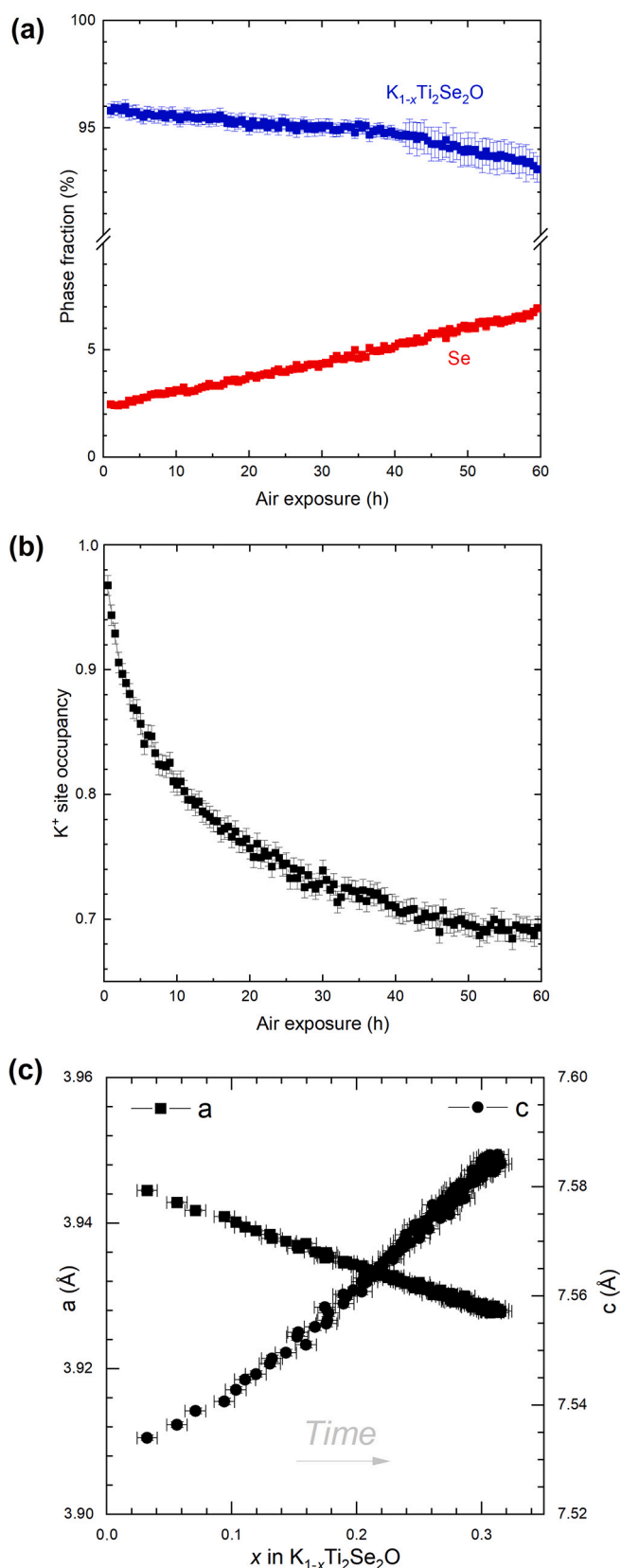


Fig. 4. Results of air exposure on $\text{KTi}_2\text{Se}_2\text{O}$. (a) Phase fractions of $\text{K}_{1-x}\text{Ti}_2\text{Se}_2\text{O}$ and Se as a function of time. (b) Refined potassium site fractional occupancy as a function of time. (c) Relationships between the potassium stoichiometry and lattice parameters of $\text{K}_{1-x}\text{Ti}_2\text{Se}_2\text{O}$; note non-linear dependence on air exposure time.

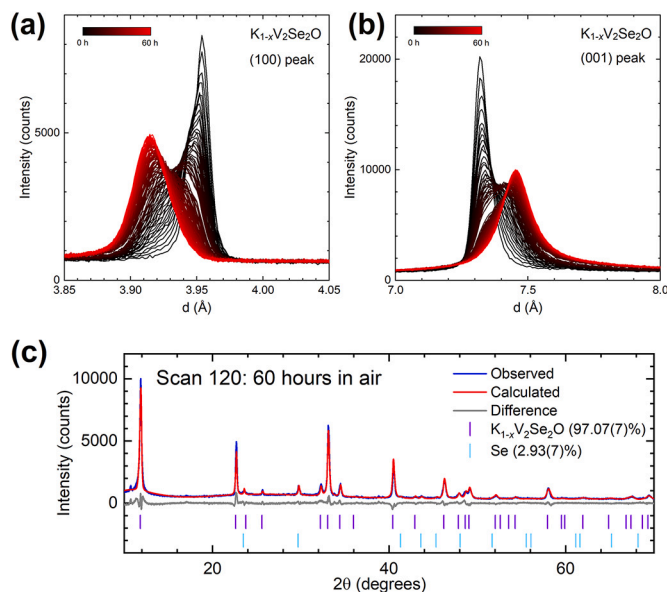


Fig. 5. (a),(b): PXRD data for $K_{1-x}V_2Se_2O$ at 0–60 hours exposure to moist air. (c) Rietveld refinement after 60 hours air exposure. Blue lines: observed intensities, red: calculated, grey: difference. Tick marks show the positions of Bragg reflections.

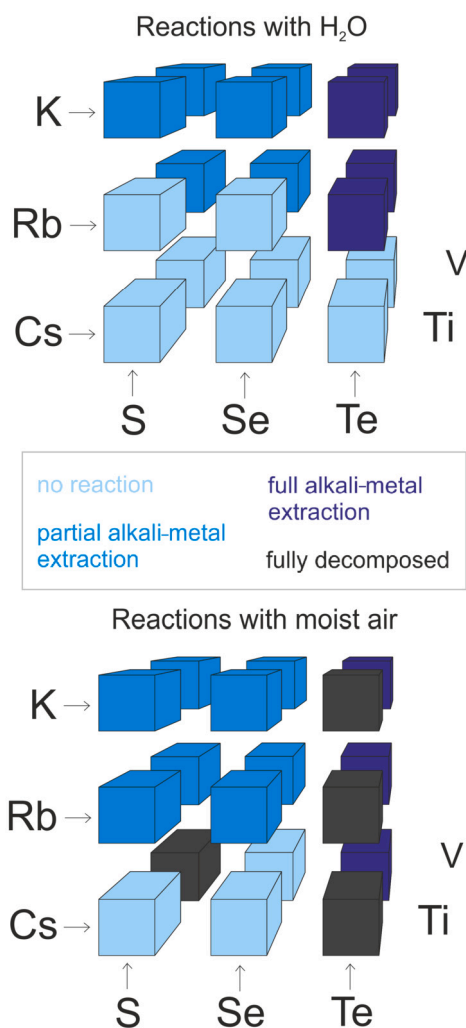


Fig. 6. Illustration highlighting the different reactivity of the AM_2Q_2O materials with H_2O under an inert atmosphere (top) or with moist air (bottom).

temperature. However, two-probe measurements at room temperature indicated that all compositions of AM_2Q_2O with $M = V$ contain itinerant electrons, with resistances of the order of $1\ \Omega$ for sintered pellets of diameter 5 mm and thickness 0.4–1.0 mm, i.e. resistivities of 10^0 to $10^2\ \Omega\ cm$ (Table S3). This is consistent with previous measurements on samples in this series [13–16] and is unsurprising given the colour of the samples (black) and the chemical compositions and oxidation states involved. The relatively large resistivities might also be related to lower compactness of the pellets and/or higher concentration of grain boundaries compared with literature reports. The average oxidation state of the transition metals (M) in AM_2Q_2O is +2.5 for the stoichiometric 1221 composition, increasing to +3 in the alkali metal-free van der Waals materials [14,16]. The M ions occupy a single crystallographic site and are therefore assumed to be indistinguishable [44], consistent with electronic delocalisation and high conductivity in the mixed-valent cases [13–16].

Magnetic susceptibility data are presented in Fig. 7. Consistent with the electronic behaviour, the susceptibility measurements showed bulk temperature-independent paramagnetism (TIP) below room temperature with a low-temperature Curie tail at $T < 50\ K$ from paramagnetic impurities. Assuming that only spin- $\frac{1}{2}$ impurities were present, the amounts of these were estimated (by fitting to $\chi = \chi_0 + C/T$) as 0.002 to 0.07 moles of $S = \frac{1}{2}$ ions per mole of sample. Small anomalies at $T = 50\ K$ are ascribed to the presence of small amounts of molecular oxygen [45] in the magnetometer, observable because of the low magnetic moment of the samples, and the subtle anomalies at $T \approx 170\ K$ in some vanadium-containing compositions correspond to the V_2O_3 impurity phase (Fig. S15 and [16,46]). The magnitude of the susceptibility is of the order 10^{-4} to 10^{-2} , in line with literature results [13–16], but quantitative trends with respect to A , M or Q cannot be established owing to the presence of impurity phases.

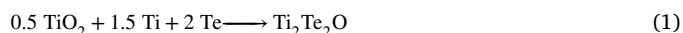
3.5. Synthesis, structure and properties of Ti_2Te_2O

A new layered oxide telluride, Ti_2Te_2O , was synthesised by reacting either KTi_2Te_2O or $RbTi_2Te_2O$ with deionised water under an inert atmosphere. During this topochemical reaction, the layers of edge-sharing TiO_2Te_4 octahedra remain intact but shift relative to one another, such that Ti_2Te_2O is body-centered ($I4/mmm$) as opposed to the primitive symmetry of the parent materials. The process is illustrated in Fig. 8(a). The product Ti_2Te_2O is isostructural with V_2Te_2O which was reported in 2018 following a similar synthetic route [36]. The lattice parameters of Ti_2Te_2O were $a = 4.04811(5)\ \text{\AA}$ and $c = 13.3891(2)\ \text{\AA}$, which are respectively 3 and 1% larger than the corresponding values for V_2Te_2O [36].

Side reactions occurred during the synthesis to produce Te and Ti_2O_3 , reflecting the ease of oxidation of telluride and titanium. A representative refinement is given in Fig. 8(b). A maximum of around 80 wt% Ti_2Te_2O could be achieved under different reaction conditions: parent material, temperature, time, and scale (Table S1). We could also produce Ti_2Te_2O in lower purity by using I_2 to remove Cs from $CsTi_2Te_2O$ [15]. 1 mol of $CsTi_2Te_2O$ was reacted with 1 mol of iodine in anhydrous THF at $60\ ^\circ C$ for 3 days in a Schlenk tube under flowing N_2 . The product was filtered, washed twice with degassed H_2O to remove CsI , then washed twice with THF and dried under vacuum to leave $Ti_2Te_2O + Te$ (Fig. S11).

Air-exposure studies on Ti_2Te_2O (carried out *ex situ* over 24 h as described in section 3.3) showed that it decomposes slowly in moist air. This suggests that oxygen is key to the decomposition. The peaks for impurity phases did not increase in intensity during this time, and the background curve changed shape (Fig. 9), indicating that the decomposition produces amorphous products.

Ceramic synthesis of Ti_2Te_2O was attempted according to the following equation:



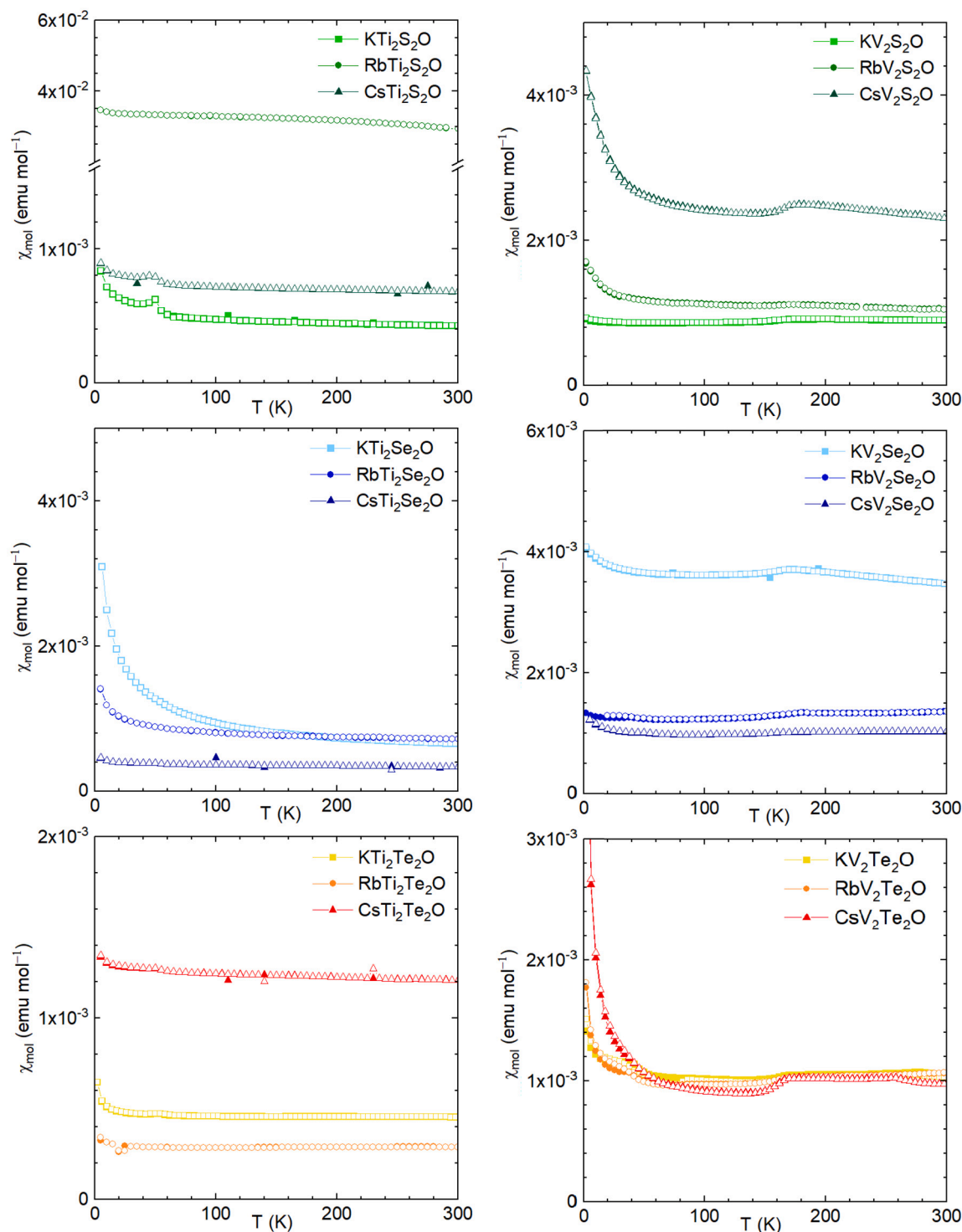


Fig. 7. Magnetic susceptibility at 1 T for AM_2Q_2O powder samples. Filled symbols: zero-field-cooled (ZFC), open symbols: field-cooled (FC).

The powdered reagents were ground together and heated in evacuated silica ampoules at 300–650 °C in steps of 50 °C, with intermediate grinding and PXRD data collection, Fig. 10. Ti_2Te_2O was not observed at any temperature. Additionally, variable-temperature synchrotron XRD on Ti_2Te_2O in a sealed capillary showed that it exhibits positive thermal expansion, with a small change of gradient around 250–260 K, Fig. 11(a) which could indicate a subtle electronic transition. Refinements below 250 K showed no extra peaks or evidence for structural distortions, e.g. to an orthorhombic unit cell. On heating, Ti_2Te_2O then gradually decomposed into $TiTe_2$ + Ti_2O_3 over the tem-

perature range 600–700 K (Figures S12–S14). The results indicate that Ti_2Te_2O is a metastable compound, like V_2Te_2O , which was also inaccessible using ceramic methods and which decomposed at $T \approx 775$ K [36].

Finally, the magnetic susceptibility of Ti_2Te_2O powder samples was measured, Fig. 11(b). Different samples showed qualitatively similar behaviour. After a low-temperature Curie tail and a small bump at 50 K from molecular oxygen [45], the susceptibility appeared temperature-independent before increasing at around 250 K. The main secondary phases, Te and Ti_2O_3 , are diamagnetic and paramagnetic respectively

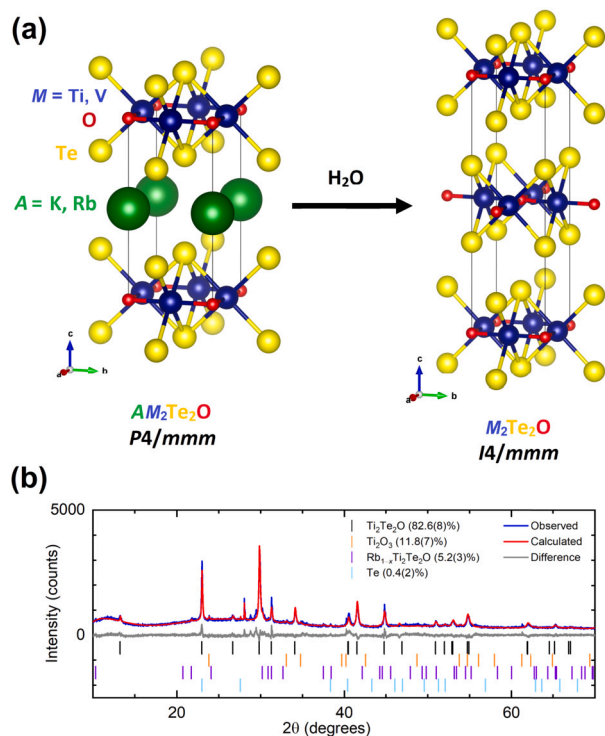


Fig. 8. (a) Schematic illustrating the topochemical synthesis of the layered van der Waals compounds V_2Te_2O [36] and Ti_2Te_2O . (b) Rietveld refinement of PXRD data for Ti_2Te_2O produced from $RbTi_2Te_2O + H_2O$. Blue lines: observed intensities, red: calculated, grey: difference.

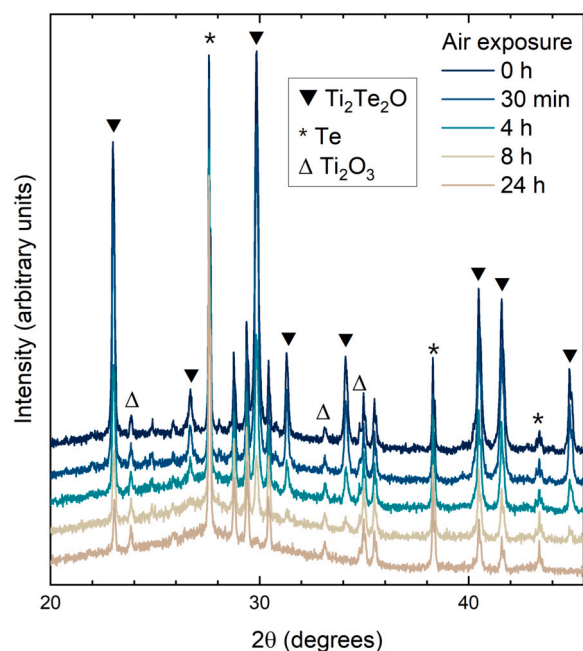


Fig. 9. Controlled air exposure on a sample of Ti_2Te_2O .

(Figures S16 and S17), and the transition temperature (which is consistent from sample to sample, see Fig. 11(b)) matches that of the change in gradient of dV/dT , so the feature is assumed to be intrinsic to Ti_2Te_2O . More detailed magnetic and electronic characterisation will require samples free of any secondary phases and ideally single crystals to investigate the fundamental electronic properties of this 2D van der Waals system.

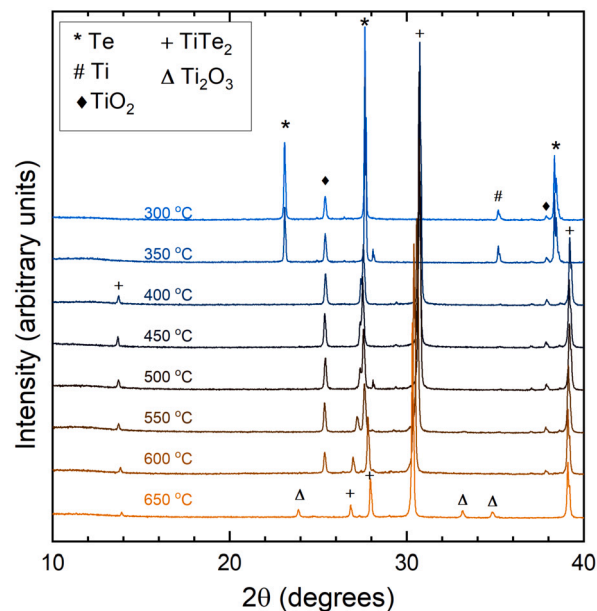


Fig. 10. Laboratory PXRD data during the attempted ceramic synthesis of Ti_2Te_2O .

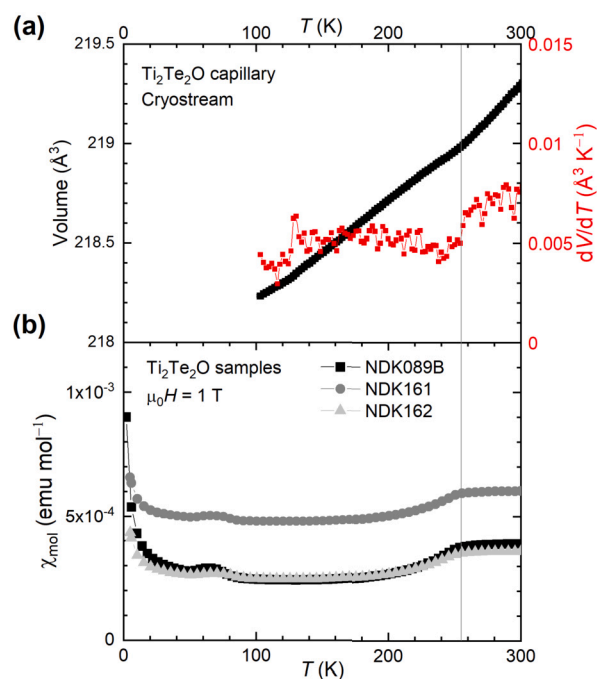


Fig. 11. (a) Unit cell volume of Ti_2Te_2O from sequential Rietveld refinement of variable-temperature synchrotron PXRD data. (b) ZFC magnetic susceptibility at 1 T for samples of Ti_2Te_2O . The vertical line at 255 K indicates a possible transition.

4. Conclusion

We have reported the solid-state synthesis of thirteen new oxide chalcogenides with the general formula AM_2Q_2O , where $A = K/Rb/Cs$, $M = Ti/V$, and $Q = S/Se/Te$. We also synthesised the other five previously reported compounds in this family and measured their structures and physical properties. This enabled us to determine the trends in compositional range, structural parameters and reactivity across the whole series as a function of alkali metal, transition metal and chalcogenide. The AM_2Q_2O oxide chalcogenides are air- and water-sensitive to different extents: for example, exposure of KTi_2Se_2O to H_2O causes partial

deintercalation of K^+ ions to give $K_{1-x}Ti_2Se_2O$, $0 \leq x \leq 0.3$, whereas $RbTi_2Se_2O$ was found to be inert to H_2O in the absence of oxygen. The AM_2Q_2O materials conduct electricity well and display temperature-independent paramagnetism, suggestive of metallic behaviour which is consistent with the behaviour of low-valent early transition metal systems. We were unable to synthesise the $M = Cr$ analogues.

We carried out soft chemical reactions on the AM_2Q_2O oxide chalcogenides, finding that V_2Te_2O can be obtained not only from RbV_2Te_2O [36] but also from KV_2Te_2O by reaction with deoxygenated H_2O . Furthermore, a new van der Waals compound Ti_2Te_2O , isostructural with V_2Te_2O , can be obtained by reaction of either KTi_2Te_2O or $RbTi_2Te_2O$ with water at room temperature, or from $CsTi_2Te_2O + I_2$ at $60^\circ C$. Far fewer oxide tellurides have been reported than oxide sulfides or selenides [19]. Our discovery significantly extends the number of known ternary oxide tellurides, which to our knowledge were previously limited to V_2Te_2O [36] and M_2O_2Te with $M = La, Ce$ or Pr [19]. Monolayers of Ti_2Te_2O have been predicted to be semimetallic and to host unusual quantum Hall states depending on the type of magnetic order [47], while the hypothetical van der Waals compound V_2S_2O offers an intriguing target phase which has been proposed for potassium-ion battery applications [48]. Therefore, further studies should be carried out on the soft chemistry of these layered mixed-anion phases, with a particular focus on the synthesis of high-quality single crystal and/or thin film samples for detailed physical property measurements.

CRediT authorship contribution statement

Nicola D. Kelly: Conceptualization, Formal analysis, Investigation, Visualization, Writing – original draft. **Simon J. Clarke:** Funding acquisition, Supervision, Writing – review & editing.

Declaration of competing interest

The authors declare the following financial interests/personal relationships which may be considered as potential competing interests: Simon J Clarke reports financial support was provided by Engineering and Physical Sciences Research Council. Former Associate Editor of Journal (2012-2019) - SJC.

Data availability

Data will be made available on request.

Acknowledgements

We acknowledge funding from the UK EPSRC (EP/T027991/1) and the Diamond Light Source (Block Allocation Grant CY25166). We thank Dr Simon Cassidy, Dr Viktoria Falkowski, Mr Robert Smyth, Mr Souvik Giri and Mr James Murrell for assistance on the I11 beamline.

Appendix A. Supplementary material

Supplementary data associated with this article can be found in the online version at <https://doi.org/10.1016/j.jssc.2023.124276>.

References

- [1] H. Kageyama, K. Hayashi, K. Maeda, J.P. Attfield, Z. Hiroi, J.M. Rondinelli, K.R. Poeppelmeier, Expanding frontiers in materials chemistry and physics with multiple anions, *Nat. Commun.* 9 (2018) 772, <https://doi.org/10.1038/s41467-018-02838-4>.
- [2] J.K. Harada, N. Charles, K.R. Poeppelmeier, J.M. Rondinelli, Heteroanionic materials by design: progress toward targeted properties, *Adv. Mater.* 31 (2019) 1805295, <https://doi.org/10.1002/adma.201805295>.
- [3] M. Orr, G.R. Hebbard, E.E. McCabe, R.T. Macaluso, Structural diversity of rare-Earth oxychalcogenides, *ACS Omega* 7 (2022) 8209–8218, <https://doi.org/10.1021/acsomega.2c00186>.
- [4] S.J. Clarke, P. Adamson, S.J.C. Herkelrath, O.J. Rutt, D.R. Parker, M.J. Pitcher, C.F. Smura, Structures, physical properties, and chemistry of layered oxychalcogenides and oxypnictides, *Inorg. Chem.* 47 (19) (2008) 8473–8486, <https://doi.org/10.1021/ic8009964>.
- [5] M. Valldor, Anion ordering in bichalcogenides, *Inorganics* 4 (2016) 23, <https://doi.org/10.3390/inorganics4030023>.
- [6] J. Gamon, A.J. Perez, L.A. Jones, M. Zanella, L.M. Daniels, R.E. Morris, C.C. Tang, T.D. Veal, L.J. Hardwick, M.S. Dyer, J.B. Claridge, M.J. Rosseinsky, $Na_2Fe_2OS_2$, a new Earth abundant oxysulphide cathode material for Na-ion batteries, *J. Mater. Chem. A* 8 (39) (2020) 20553–20569, <https://doi.org/10.1039/d0ta07966a>.
- [7] J.N. Blandy, D.R. Parker, S.J. Cassidy, D.N. Woodruff, X. Xu, S.J. Clarke, Synthesis, structure, and compositional tuning of the layered oxide tellurides $Sr_2MnO_2Cu_{2-x}Te_2$ and $Sr_2CoO_2Cu_2Te_2$, *Inorg. Chem.* 58 (12) (2019) 8140–8150, <https://doi.org/10.1021/acs.inorgchem.9b00919>.
- [8] Y. Fuwa, M. Wakeshima, Y. Hinatsu, Crystal structure and magnetic properties of a new layered cobalt oxyselenide $La_2Co_2O_3Se_2$, *Solid State Commun.* 150 (35–36) (2010) 1698–1701, <https://doi.org/10.1016/j.ssc.2010.06.016>.
- [9] N. Ni, E. Climent-Pascual, S. Jia, Q. Huang, R.J. Cava, Physical properties and magnetic structure of the layered oxyselenide $La_2O_3Mn_2Se_2$, *Phys. Rev. B, Condens. Matter Mater. Phys.* 82 (2010) 214419, <https://doi.org/10.1103/PhysRevB.82.214419>.
- [10] Z.A. Gál, O.J. Rutt, C.F. Smura, T.P. Overton, N. Barrier, S.J. Clarke, J. Hadermann, Structural chemistry and metamagnetism of an homologous series of layered manganese oxysulfides, *J. Am. Chem. Soc.* 128 (26) (2006) 8530–8540, <https://doi.org/10.1021/ja060892o>.
- [11] T. Yajima, K. Nakano, F. Takeiri, T. Ono, Y. Hosokoshi, Y. Matsushita, J. Hester, Y. Kobayashi, H. Kageyama, Superconductivity in $BaTi_2Sb_2O$ with a d^1 square lattice, *J. Phys. Soc. Jpn.* 81 (2012) 103706, <https://doi.org/10.1143/JPSJ.81.103706>.
- [12] T. Yajima, K. Nakano, F. Takeiri, J. Hester, T. Yamamoto, Y. Kobayashi, N. Tsuji, J. Kim, A. Fujiwara, H. Kageyama, Synthesis and physical properties of the new oxysulfides $BaTi_2Bi_2O$ and $(SrF)_2Ti_2Bi_2O$ with a d^1 square net, *J. Phys. Soc. Jpn.* 82 (2013) 013703, <https://doi.org/10.7566/JPSJ.82.013703>.
- [13] M. Valldor, P. Merz, Y. Prots, W. Schnelle, Bad-metal-layered sulfide oxide CsV_2S_2O , *Eur. J. Inorg. Chem.* 2016 (1) (2016) 23–27, <https://doi.org/10.1002/ejic.201501154>.
- [14] M. Valldor, P. Merz, Y. Prots, Y. Watier, W. Schnelle, Synthesis and characterization of $Cs_{1-x}Ti_2Te_2O$ ($x \approx 0.2$): electron doping by Te resulting in a layered metal, *Inorg. Chem.* 55 (21) (2016) 11337–11341, <https://doi.org/10.1021/acs.inorgchem.6b01903>.
- [15] H. Lin, J. Si, X. Zhu, K. Cai, H. Li, L. Kong, X. Yu, H.H. Wen, Structure and physical properties of $CsV_2Se_{2-x}O$ and V_2Se_2O , *Phys. Rev. B* 98 (2018) 075132, <https://doi.org/10.1103/PhysRevB.98.075132>.
- [16] A. Abiliti, Y.L. Sun, H. Jiang, S.Q. Wu, Y.B. Liu, G.H. Cao, Weak metal-metal transition in the vanadium oxytelluride $Rb_{1-x}V_2Te_2O$, *Phys. Rev. B* 97 (2018) 214517, <https://doi.org/10.1103/PhysRevB.97.214517>.
- [17] Z. Guo, F. Sun, D. Puggioni, Y. Luo, X. Li, X. Zhou, D.Y. Chung, E. Cheng, S. Li, J.M. Rondinelli, W. Yuan, M.G. Kanatzidis, Local distortions and metal-semiconductor-metal transition in quasi-one-dimensional nanowire compounds $AV_3Q_3O_6$ ($A = K, Rb, Cs$ and $Q = Se, Te$), *Chem. Mater.* 33 (7) (2021) 2611–2623, <https://doi.org/10.1021/acs.chemmater.1c00434>.
- [18] S.-J. Song, Y.-Q. Lin, B.-Z. Li, S.-Q. Wu, Q.-Q. Zhu, Z. Ren, G.-H. Cao, Tetragonal polymorph of $BaFe_2S_2O$ as an antiferromagnetic Mott insulator, *Phys. Rev. Mater.* 6 (2022) 055002, <https://doi.org/10.1103/PhysRevMaterials.6.055002>.
- [19] M.S. Orr, K.R. Cruz, H.H. Nguyen, A.L. Kojima, R.T. Macaluso, Versatility of tellurium in heteroanionic Ln_2O_2Te ($Ln = La, Ce, Pr$) and tellurate Ln_2TeO_6 ($Ln = La, Pr$), *Inorg. Chem.* 61 (2022) 18002–18009, <https://doi.org/10.1021/acs.inorgchem.2c02287>.
- [20] M. Wintemberger, J. Dugue, M. Guittard, N.H. Dung, V. Tien, Ferro- and antiferromagnetism in oxychalcogenides $LnCrOX_2$ ($Ln = La$ or Nd and $X = S$ or Se), *J. Solid State Chem.* 70 (2) (1987) 295–302, [https://doi.org/10.1016/0022-4596\(87\)90068-5](https://doi.org/10.1016/0022-4596(87)90068-5).
- [21] X.F. Wang, Y.J. Yan, J.J. Ying, Q.J. Li, M. Zhang, N. Xu, X.H. Chen, Structure and physical properties for a new layered pnictide-oxide: $BaTi_2As_2O$, *J. Phys. Condens. Matter* 22 (2010) 075702, <https://doi.org/10.1088/0953-8984/22/7/075702>.
- [22] T. Yajima, K. Nakano, F. Takeiri, Y. Nozaki, Y. Kobayashi, H. Kageyama, Two superconducting phases in the isovalent solid solutions $BaTi_2Pn_2O$ ($Pn = As, Sb$, and Bi), *J. Phys. Soc. Jpn.* 82 (2013) 033705, <https://doi.org/10.7566/JPSJ.82.033705>.
- [23] P. Doan, M. Goch, Z. Tang, B. Lorenz, A. Mo, J. Tapp, $Ba_{1-x}Na_xTi_2Sb_2O$ ($0.0 \leq x \leq 0.33$): a layered titanium-based pnictide oxide superconductor, *J. Am. Chem. Soc.* 134 (2012) 16520–16523.
- [24] U. Pachmayr, D. Johrendt, Superconductivity in $Ba_{1-x}K_xTi_2Sb_2O$ ($0 \leq x \leq 1$) controlled by the layer charge, *Solid State Sci.* 28 (2014) 31–34, <https://doi.org/10.1016/j.solidstatesciences.2013.12.005>.
- [25] F. von Rohr, R. Nesper, A. Schilling, Superconductivity in rubidium-substituted $Ba_{1-x}Rb_xTi_2Sb_2O$, *Phys. Rev. B, Condens. Matter Mater. Phys.* 89 (2014) 094505, <https://doi.org/10.1103/PhysRevB.89.094505>.
- [26] Y. Wang, X. Yang, T. Taguchi, H. Li, T. He, H. Goto, R. Eguchi, T. Miyazaki, Y.F. Liao, H. Ishii, Y. Kubozono, Preparation and characterization of superconducting $Ba_{1-x}Cs_xTi_2Sb_2O$, and its pressure dependence of superconductivity, *Jpn. J. Appl. Phys.* 58 (2019) 110603, <https://doi.org/10.7567/1347-4065/ab4ef5>.

- [27] H. Kabbour, E. Janod, B. Corraze, M. Danot, C. Lee, M.H. Whangbo, L. Cario, Structure and magnetic properties of oxychalcogenides $A_2F_2Fe_2OQ_2$ ($A = \text{Sr, Ba}$; $Q = \text{S, Se}$) with Fe_2O square planar layers representing an antiferromagnetic checkerboard spin lattice, *J. Am. Chem. Soc.* 130 (26) (2008) 8261–8270, <https://doi.org/10.1021/ja711139g>.
- [28] Y. Fuwa, M. Wakeshima, Y. Hinatsu, Crystal structure, magnetic properties, and Mössbauer spectroscopy of new layered iron oxyselenide $Nd_2Fe_2O_3Se_2$, *J. Phys. Condens. Matter* 22 (2010) 346003, <https://doi.org/10.1088/0953-8984/22/34/346003>.
- [29] J.M. Mayer, L.F. Schneemeyer, T. Siegrist, J.V. Waszczak, B. Van Dover, New layered iron-lanthanum-oxide-sulfide and -selenide phases: $Fe_2La_2O_3E_2$ ($E = \text{S, Se}$), *Angew. Chem., Int. Ed.* 31 (12) (1992) 1645–1647.
- [30] J.B. He, D.M. Wang, H.L. Shi, H.X. Yang, J.Q. Li, G.F. Chen, Synthesis, structure, and magnetic properties of the layered iron oxychalcogenide $Na_2Fe_2Se_2O$, *Phys. Rev. B, Condens. Matter Mater. Phys.* 84 (2011) 205212, <https://doi.org/10.1103/PhysRevB.84.205212>.
- [31] N. Ni, S. Jia, Q. Huang, E. Climent-Pascual, R.J. Cava, Structural, transport, thermodynamic, and neutron diffraction studies of layered $R_2O_3Fe_2Se_2$ ($R = \text{Ce, Pr, Nd, and Sm}$), *Phys. Rev. B, Condens. Matter Mater. Phys.* 83 (2011) 224403, <https://doi.org/10.1103/PhysRevB.83.224403>.
- [32] D.G. Free, N.D. Withers, P.J. Hickey, J.S. Evans, Synthesis, structure and properties of several new oxychalcogenide materials with the general formula $A_2O_3M_2OSe_2$ ($A = \text{La-Sm}$, $M = \text{Fe, Mn}$), *Chem. Mater.* 23 (6) (2011) 1625–1635, <https://doi.org/10.1021/cm1035453>.
- [33] F. Takeiri, Y. Matsumoto, T. Yamamoto, N. Hayashi, Z. Li, T. Tohyama, C. Tassel, C. Ritter, Y. Narumi, M. Hagiwara, H. Kageyama, High-pressure synthesis of the layered iron oxyselenide $BaFe_2Se_2O$ with strong magnetic anisotropy, *Phys. Rev. B* 94 (2016) 184426, <https://doi.org/10.1103/PhysRevB.94.184426>.
- [34] B.D. Coles, A.D. Hillier, F.C. Coomer, N.C. Bristowe, S. Ramos, E.E. McCabe, Spin interactions and magnetic order in the iron oxychalcogenides $BaFe_2Q_2O$ ($Q = \text{S and Se}$), *Phys. Rev. B* 100 (2019) 024427, <https://doi.org/10.1103/PhysRevB.100.024427>.
- [35] B.C. Sheath, X. Xu, P. Manuel, J. Hadermann, M. Batuk, J. O'Sullivan, R.S. Bonilla, S.J. Clarke, Structures and magnetic ordering in layered Cr oxide arsenides $Sr_2CrO_2Cr_2OAs_2$ and Sr_2CrO_3CrAs , *Inorg. Chem.* 61 (31) (2022) 12373–12385, <https://doi.org/10.1021/acs.inorgchem.2c01773>.
- [36] A. Ablimit, Y.L. Sun, E.J. Cheng, Y.B. Liu, S.Q. Wu, H. Jiang, Z. Ren, S. Li, G.H. Cao, V_2Te_2O : a two-dimensional van der Waals correlated metal, *Inorg. Chem.* 57 (23) (2018) 14617–14623, <https://doi.org/10.1021/acs.inorgchem.8b02280>.
- [37] S.P. Thompson, J.E. Parker, J. Potter, T.P. Hill, A. Birt, T.M. Cobb, F. Yuan, C.C. Tang, Beamline I11 at diamond: a new instrument for high resolution powder diffraction, *Rev. Sci. Instrum.* 80 (2009) 075107, <https://doi.org/10.1063/1.3167217>.
- [38] H.M. Rietveld, A profile refinement method for nuclear and magnetic structures, *J. Appl. Crystallogr.* 2 (1969) 65–71, <https://doi.org/10.1107/S0021889869006558>.
- [39] A.A. Coelho, TOPAS and TOPAS-academic: an optimization program integrating computer algebra and crystallographic objects written in C++, *J. Appl. Crystallogr.* 51 (2018) 210–218, <https://doi.org/10.1107/S1600576718000183>.
- [40] X. Wei, M. Akinc, Crystal structure analysis of Si- and Zn-codoped tricalcium phosphate by neutron powder diffraction, *J. Am. Ceram. Soc.* 90 (2007) 2709.
- [41] T. Ohtani, Y. Miyoshi, Y. Fujii, T. Koyakumaru, T. Kusano, K. Minami, Superconductivity and phase transition in quasi-one-dimensional sulfide AV_6S_8 ($A = \text{In, Tl, K, Rb, Cs}$), *Solid State Commun.* 120 (2001) 95–99.
- [42] S. Jöbic, R. Brec, J. Rouxel, Anionic polymeric bonds in transition metal ditellurides, *J. Solid State Chem.* 96 (1) (1992) 169–180, [https://doi.org/10.1016/S0022-4596\(05\)80309-3](https://doi.org/10.1016/S0022-4596(05)80309-3).
- [43] T.C. Ozawa, T. Naka, A. Matsushita, S.M. Kauzlarich, T. Sasaki, Chemical composition and magnetic property modifications of $Na_2Ti_2Sb_2O$ using PTFE as an alkali-metal ion extraction reagent, *J. Fluorine Chem.* 168 (2014) 189–192, <https://doi.org/10.1016/j.jfluchem.2014.09.028>.
- [44] M.B. Robin, P. Day, Mixed valence chemistry - a survey and classification, *Adv. Inorg. Chem. Radiochem.* 10 (1968) 274–422, [https://doi.org/10.1016/S0065-2792\(08\)60179-X](https://doi.org/10.1016/S0065-2792(08)60179-X).
- [45] C. Uyeda, K. Sugiyama, M. Date, High field magnetization of solid oxygen, *J. Phys. Soc. Jpn.* 54 (1985) 1107.
- [46] D. Adler, Mechanisms for metal-nonmetal transitions in transition-metal oxides and sulfides, *Rev. Mod. Phys.* 40 (4) (1968) 714–736, <https://doi.org/10.1103/RevModPhys.40.714>.
- [47] H.-Y. Ma, D. Guan, S. Wang, Y. Li, C. Liu, H. Zheng, J.-F. Jia, Quantum spin Hall and quantum anomalous Hall states in magnetic Ti_2Te_2O single layer, *J. Phys. Condens. Matter* 33 (2021) 21LT01, <https://doi.org/10.1088/1361-648X/abe647>.
- [48] Y.X. Yu, High storage capacity and small volume change of potassium-intercalation into novel vanadium oxychalcogenide monolayers V_2S_2O , V_2Se_2O and V_2Te_2O : an ab initio DFT investigation, *Appl. Surf. Sci.* 546 (2021) 149062, <https://doi.org/10.1016/j.apsusc.2021.149062>.